Hadronic production of top-quark pairs in association with a pair of leptons in the POWHEG BOX framework

Margherita Ghezzi,* Barbara Jäger,† and Santiago Lopez Portillo Chavez‡
Institute for Theoretical Physics, University of Tübingen, Auf der Morgenstelle 14, 72076 Tübingen, Germany

Laura Reina§
Physics Department, Florida State University, Tallahassee, Florida 32306-4350, USA

Doreen Wackeroth‖
Department of Physics, University at Buffalo, The State University of New York, 239 Fronczak Hall, Buffalo, New York 14221, USA

(Received 21 December 2021; accepted 2 June 2022; published 1 July 2022)

We present an implementation of $t\bar{t}\ell^+\ell^-$ ($\ell = e, \mu$) hadronic production at next-to-leading order in QCD matched to parton-shower event generators in the POWHEG BOX framework. The program we developed includes all leading-order contributions of order $\alpha_s^2\alpha^2$ for the specified final state, as well as the corresponding first-order QCD corrections. Decays of the top quarks have been simulated retaining spin-correlations in all tree-level matrix elements. We consider the case of the Large Hadron Collider at $\sqrt{s} = 13$ TeV and compare results for $t\bar{t}\ell^+\ell^-$ production in the fiducial volume where the invariant mass of the lepton pairs is centered around the Z-boson mass to corresponding predictions for $t\bar{t}Z$ on-shell production with $Z \to \ell^+\ell^-$. We find that off-shell effects in $t\bar{t}\ell^+\ell^-$ are in general small at the level of the total cross section, but can decrease the tail of the leptons' transverse momentum distributions by 10%–20% and, in these regions, they are visible beyond the scale uncertainty due to renormalization and factorization scale variation. Moreover, we find that accounting for top-quark decays in the narrow-width approximation with tree-level spin correlations also gives origin to 10%–20% effects in specific regions of the kinematic distributions of the $t\bar{t}\ell^+\ell^-$ decayed final state.

DOI: 10.1103/PhysRevD.106.014001

I. INTRODUCTION

The CERN Large Hadron Collider (LHC) provides energies and luminosities high enough to produce an unprecedented number of top quarks. As a top-quark factory, it constitutes an ideal environment for exploring the properties of the heaviest known elementary fermion to date. While several intrinsic properties of the top quark are accessible in top-quark pair production ($pp \to t\bar{t}$), the production of top quarks with electroweak (EW) massive gauge bosons (tW as well as $t\bar{t} + V$ for $V = W^\pm, Z$) strongly probes the consistency of the Standard Model (SM) through a comprehensive set of top-quark production measurements and can be crucial to constrain new physics beyond the SM. In particular, while single top-production (tW) gives access to the top-quark coupling to $W^\pm$ bosons, its coupling to the Z boson can best be probed in $t\bar{t}Z$ associated production. At the same time, the production of $t\bar{t}W^\pm$ and $t\bar{t}Z$ are important backgrounds in the measurement of the associated production of the Higgs boson with a top quark pair ($pp \to t\bar{t}H$) as well as more generally in searches of new physics which involve final states with multiple leptons and b jets.

Cross sections for the $t\bar{t}W^\pm$ and $t\bar{t}Z$ production processes measured at the LHC with center-of-mass energy $\sqrt{s} = 13$ GeV by the ATLAS [1–3] and CMS experiments [4,5] tend to be in agreement with SM expectations, but are plagued by relatively large statistical and systematic uncertainties. A crucially limiting factor in the analyses is due to theoretical uncertainties. The expected improvement of experimental accuracy in the upcoming LHC Run 3 and the future LHC high-luminosity run (HL-LHC) will unfold

*margherita.ghezzi@itp.uni-tuebingen.de
†jaeger@itp.uni-tuebingen.de
‡santiago.lopez-portillo-chavez@uni-tuebingen.de
§reina@hep.fsu.edu
‖dw24@buffalo.edu

its full potential only if accompanied by a corresponding improvement in the precision of theoretical predictions and simulation tools.

Providing the means to identify effects of new physics in deviations of measurements from SM expectations not only requires precise theoretical predictions for benchmark observables in the context of the SM and representative scenarios for its extensions, but also a realistic assessment of systematic uncertainties in experimental analyses and theoretical calculations. Such uncertainties include unknown perturbative corrections (beyond the orders in the strong and electroweak couplings considered in a calculation), nonperturbative effects (which are typically estimated using some generic models), and intrinsic uncertainties of the simulation programs used. In particular the latter can only be quantified by a comparison of conceptually different implementations.

Several precise predictions and simulation tools for the hadronic production of top-quark pairs in association with weak gauge bosons are available. Results for the corresponding total and differential cross sections including next-to-leading order (NLO) QCD and EW corrections have been presented in [6–11] for $t\bar{t}W^{\pm}$ and in [8,9,12,13] for $t\bar{t}Z$, respectively.[1] Soft-gluon resummation effects up to next-to-next-to-leading logarithms (NNLL) have been studied in [15–21]. Furthermore, the modeling of $t\bar{t}W^{\pm}$ and $t\bar{t}Z$ events have been improved by interfacing fixed-order NLO QCD calculations with parton showers (PS) in several studies [7,11,22–25] based either on the POWHEG [26,27] or MC@NLO [28,29] methods. Some of these frameworks also provide extra functionalities such as the simulation of top-quark decays including spin correlations at leading order (LO) accuracy [11,23–25] and a systematic treatment of higher jet multiplicities via multijet merging techniques [11,24].

Calculations also exist which take NLO QCD effects and off-shell effects in the decays of the top quarks and/or $W^{\pm}$ bosons into account [6,30–33]. While fixed-order NLO QCD corrections in both production and decay of the top quarks and Z boson have been taken into account for instance in [34–36], a full study of off-shell effects in the Z boson's decay modes to charged fermions is still missing. It is our goal in this paper to study the $pp \to t\bar{t}\ell^+\ell^-$ process (with $\ell^{\pm}$ denoting either $e^{\pm}$ or $\mu^{\pm}$) including both resonant and nonresonant Z- and photon-induced contributions, and explore their impact on experimentally accessible quantities such as angular correlations of the decay leptons ℓ^+ and ℓ^-. Our study includes all LO contributions of order $\alpha_s^2\alpha^2$ for the specified final state, as well as the corresponding first-order QCD corrections. Moreover, we aim at presenting a dedicated Monte Carlo program allowing not only the calculation of NLO QCD corrections to the $pp \to t\bar{t}\ell^+\ell^-$ production process, but also providing the option of taking into account decays of the top quarks with full tree-level spin correlations in the narrow-width approximation, using the method of Ref. [37].

Furthermore we have implemented the NLO QCD calculation of this process in POWHEG BOX [38], which provides an interface to general-purpose Monte Carlo PS event generators such as PYTHIA and HERWIG using the POWHEG method [26,27]. For completeness, we have also developed an independent implementation of $pp \to t\bar{t}Z$ at NLO QCD matched to PS using the POWHEG method in POWHEG BOX, and will describe the implementation of both processes in the course of this paper. We notice that for the first time the implementation of both processes will be available as part of the POWHEG BOX-V2 repository, which also includes processes such as $pp \to t\bar{t}H$ [39,40]. This will allow to generate both signal and background events in a consistent framework for studies of Higgs-boson associated production with top-quark pairs. We hope that the tools described in this paper will help in the analysis and interpretation of data collected by the ATLAS and CMS experiments in upcoming LHC runs and will facilitate the study of residual modeling uncertainties [41,42].

This article is structured as follows. In the next section we explain the implementation of the $t\bar{t}\ell^+\ell^-$ production process in the POWHEG BOX framework, while detailed numerical studies are presented in Sec. III. We summarize our findings in Sec. IV.

II. IMPLEMENTATION

We consider the production of the $t\bar{t}\ell^+\ell^-$ final state in proton-proton collisions ($pp \to t\bar{t}\ell^+\ell^-$, with $\ell = e, \mu$) and calculate the corresponding cross section up to NLO in the strong coupling α_s and at LO in the EW coupling α, i.e., we consider LO contributions of order $\alpha_s^2\alpha^2$ and NLO QCD contributions of order $\alpha_s^3\alpha^2$. As illustrated in Fig. 1, both Z and photon (γ) contributions are retained and the effect of both contributions and their interference will be discussed in Sec. III. Since we assume both electrons and muons to be massless, the calculation for both cases is the same. Representative diagrams are shown in Fig. 1 for both LO contributions (top row) and real and virtual NLO QCD corrections (bottom row). As part of our study we also consider the corresponding production of an on-shell $t\bar{t}Z$ final state ($pp \to t\bar{t}Z$) followed by the Z-boson decaying into a pair of charged leptons ($Z \to \ell^+\ell^-$) and calculate it at the same perturbative order (i.e., $\mathcal{O}(\alpha_s^3\alpha)$ for $t\bar{t}Z$ production and $\mathcal{O}(\alpha_s^3\alpha^2)$ when including the decay of the Z-boson).[2]

[1] A review and comparison of fixed-order results has also been presented in the 4th report of the LHC Higgs Cross Section Working Group [14].

[2] In order to test our $pp \to t\bar{t}Z$ implementation, we compared results obtained with our code for $t\bar{t}Z$ production to results presented in Ref. [14]. Using the setup of Ref. [14], we find excellent agreement at fixed-order NLO QCD for both total and differential rates.

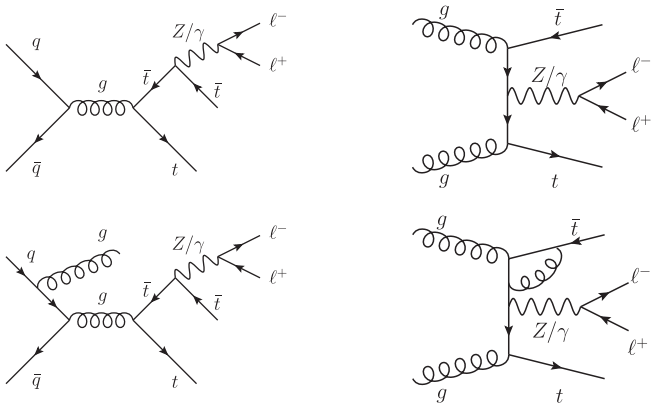

FIG. 1. Representative Feynman diagrams for quark- and gluon-induced contributions to the $pp \to t\bar{t}\ell^+\ell^-$ process. The top row illustrates examples of processes that contribute to the LO QCD cross section at order $\alpha_s^2\alpha^2$, while the bottom row provides examples of real-emission (bottom left) and virtual (bottom right) NLO QCD corrections.

For the implementation of the $pp \to t\bar{t}\ell^+\ell^-$ and $pp \to t\bar{t}Z$ processes in the framework of the V2 version of POWHEG BOX, we resort to a combination of existing tools and tailored building blocks. While POWHEG BOX provides all process-independent elements of the matching of an NLO QCD calculation to parton-shower event generators, it requires process-specific input from the developer such as the flavor structure of the given process, a parameterization of its phase space, the hard-scattering matrix elements squared at LO, the NLO virtual corrections and real-emission amplitudes squared, as well as spin- and color-correlated amplitudes for the construction of infrared subtraction terms according to the Frixione-Kunszt-Signer (FKS) scheme [43].

In order to build the required tree-level amplitudes, subtraction terms, and flavor structure for the $pp \to t\bar{t}\ell^+\ell^-$ and $pp \to t\bar{t}Z$ processes, we rely on standard features of POWHEG BOX based on MadGraph 4 [44]. We provide the required $t\bar{t}\ell^+\ell^-$ phase-space parametrization with the option of mapping the Z-boson resonance if the selected fiducial volume of a given study is limited to events where the invariant mass of a pair of opposite-sign same-flavor leptons is restricted to a narrow region around the Z-boson mass. Virtual corrections are computed with the help of the one-loop provider NLOX [45,46], where we employed the complex-mass scheme [47,48] for the $t\bar{t}\ell^+\ell^-$ calculation. The interface that ensures the correct calls of the NLOX amplitudes within POWHEG BOX, as well as the transfer of the necessary input parameters, has also been developed.

While the cross section for the $t\bar{t}Z$ production process is finite at Born level without any phase-space restrictions, the cross section for the $t\bar{t}\ell^+\ell^-$ final state exhibits a collinear singularity already at tree level because of a photon of vanishing virtuality splitting into an $\ell^+\ell^-$ pair of massless leptons, cf. the photon-exchange diagrams in Fig. 1. Experimentally, such configurations are of little interest since measurements are typically performed by imposing a cut on the invariant mass of the lepton pair ($M_{\ell^+\ell^-}$) that favors configurations where the lepton pair originates from a decaying Z boson (rather than a photon of low virtuality). To exclude this singular phase-space region, we implemented a generation cut on the invariant mass of the $\ell^+\ell^-$ pair, $M^{\min}_{\ell^+\ell^-}$, which is imposed at the level of the Born phase-space generation. In the absence of QED shower effects, any analysis cut on the invariant mass of the $\ell^+\ell^-$ system has to be chosen at least equal to $M^{\min}_{\ell^+\ell^-}$.[3] The results presented in Sec. III have been obtained with $M^{\min}_{\ell^+\ell^-} = 10$ GeV and an analysis cut of $m_Z - 10\ \text{GeV} \le M_{\ell^+\ell^-} \le m_Z + 10\ \text{GeV}$.

The most basic version of our implementation treats the top quarks as stable particles. Decays of the top quarks, for instance via the chain $t \to W^+b \to \ell'^+\nu_{\ell'}b$, can in principle be simulated in the narrow-width approximation after the event-generation stage by using the decay feature of a multipurpose Monte Carlo event generator like PYTHIA. However, such a simulation of the top-quark decays is limited to the spin-averaged case and cannot provide information on correlations between the production and decay part of the full $pp \to (\ell'^+\nu_{\ell'}b)(\ell'^-\bar{\nu}_{\ell'}b)\ell^+\ell^-$ process.

In order to partially overcome these limitations, we also introduce the possibility of retaining the correlations between production and decays of the top quarks, in the narrow-width approximation, applying the method of Ref. [37]. Implementations of this method in the context of POWHEG BOX can be found in related processes such as $t\bar{t}$ + jet and $t\bar{t}H$ production [39,49]. Inspired by these examples, we proceed as follows. In a first step, the program internally generates events at NLO QCD accuracy for $t\bar{t}\ell^+\ell^-$ final states with stable top quarks. Subsequently, decays of the top quarks into bottom quarks, leptons, and neutrinos are simulated according to a probability determined by tree-level matrix elements for $(t \to \ell'^+\nu_{\ell'}b)(\bar{t} \to \ell'^-\bar{\nu}_{\ell'}\bar{b})\ell^+\ell^-(+\text{jet})$ production. The corresponding matrix elements have been obtained with MadGraph 5 [50]. In this way, the full tree-level spin correlations between production and decay are retained in the soft and collinear regions as well as in the real-emission matrix elements. For more details on the method and its implementation in POWHEG BOX, we refer the interested reader to the original publications of Refs. [37,49].

III. NUMERICAL ANALYSIS AND RESULTS

In the following, we explore the capabilities of the program we developed and present some representative

[3]We notice that, depending on the choices made at the parton-shower and analysis level, the relation between analysis and generation cut on $M_{\ell^+\ell^-}$ could vary and the user should adapt it on a case by case basis.

phenomenological results for the LHC running at a center-of-mass energy of 13 TeV. For illustration purposes, we specialize our discussion to the case of $pp \to t\bar{t}e^+e^-$ and consider the top and anti-top decays $t \to \mu^+\nu_\mu b$ and $\bar{t} \to \mu^-\bar{\nu}_\mu \bar{b}$. As explained in Sec. II, our POWHEG BOX implementation also allows to consider other choices for the leptons coming from $t\bar{t}\ell^+\ell^-$ production and top/antitop decays, with the obvious caveat that the corresponding selection of events (i.e., the selection of the final-state fiducial volume via a set of cuts on final-state particles) needs to be modified accordingly.

The effect of NLO QCD corrections on $t\bar{t}e^+e^-$ production will be presented in Sec. III A for both total and differential distributions, considering a variety of kinematic observables. In particular, we will discuss the charge asymmetry of the $t\bar{t}$ system. In order to identify the observables that are most affected by off-shell effects and the interplay between Z and photon resonant channels in $t\bar{t}e^+e^-$ production, in Sec. III B we will compare our findings to the corresponding results obtained from $t\bar{t}Z$ on-shell production matched, in the narrow-width approximation, to the decay of the Z boson into an e^+e^- pair as simulated by the decay feature of PYTHIA, the PS Monte Carlo event generator adopted in our study, where spin-correlation effects are not taken into account. In Sec. III C we present an assessment of the effect of spin correlations in the $pp \to t\bar{t}e^+e^-$ process, where we compare the two options of top-decay modeling available in our implementation. We end the section by comparing our most complete modeling of the process, $pp \to t\bar{t}e^+e^-$ with spin-correlated top decays, against the simplest one, $pp \to t\bar{t}(Z \to e^+e^-)$ without spin-correlated top decays.

The results presented in this section have been obtained using the CT18NLO set [51] of parton distribution functions (PDF) as implemented in the LHAPDF6 library [52], corresponding to $\alpha_s(m_Z) = 0.118$ for five massless quarks. For the EW input scheme we use the G_μ scheme where the Fermi constant G_μ and the masses of the Z and W bosons (m_Z, m_W) are input parameters, and the electromagnetic coupling constant α is computed via the tree-level relation:

$$\alpha = \frac{\sqrt{2}G_\mu m_W^2}{\pi}\left(1 - \frac{m_W^2}{m_Z^2}\right).$$

For our study we choose the following values for the EW input parameters [53]:

$$m_Z = 91.1876 \text{ GeV}, \qquad m_W = 80.379 \text{ GeV},$$
$$G_\mu = 1.166378 \times 10^{-5} \text{ GeV}^{-2}. \tag{1}$$

The widths of the Z and W bosons are set to [53]:

$$\Gamma_Z = 2.4952 \text{ GeV}, \qquad \Gamma_W = 2.085 \text{ GeV}, \tag{2}$$

while for the top-quark mass and width we use [53]:

$$m_t = 172.76 \text{ GeV}, \qquad \Gamma_t = 1.42 \text{ GeV}. \tag{3}$$

We define the renormalization and factorization scales as multiples of a central scale μ_0 according to $\mu_R = \xi_R\mu_0$ and $\mu_F = \xi_F\mu_0$ with variation factors ξ_R and ξ_F, and consider both the case of a fixed central scale:

$$\mu_0 = \frac{2m_t + m_Z}{2}, \tag{4}$$

and the case of a dynamical central scale:

$$\mu_0 = \frac{M_T(e^+e^-) + M_T(t) + M_T(\bar{t})}{3}, \tag{5}$$

based on the transverse masses of the top quark and antiquark, and of the e^+e^- system, where the transverse mass $M_T(i)$ of a particle or system of particles i is obtained from its (invariant) mass m_i and transverse momentum, $p_{T,i}$, via

$$M_T(i) = \sqrt{m_i^2 + p_{T,i}^2}. \tag{6}$$

In our $t\bar{t}e^+e^-$ implementation, $M_T(e^+e^-)$ is computed from the momenta of the e^+e^- system, while in the $t\bar{t}Z$ code it is determined by the momentum and mass of the Z boson. All results in this paper include a renormalization and factorization scale uncertainty obtained by a seven-point scale variation, i.e., by independently setting the scale factors ξ_F and ξ_R to the values $\frac{1}{2}$, 1 and 2 while excluding the combinations $(\xi_F, \xi_R) = (\frac{1}{2}, 2)$ and $(\xi_F, \xi_R) = (2, \frac{1}{2})$. As we will see in Sec. III A, the two scale choices give very similar results and in presenting the results of Secs. III B and III C we will consider only the fixed scale choice of Eq. (4), unless otherwise specified. In estimating the theoretical uncertainty of the results presented in this paper we do not include PDF uncertainties since, based on studies of $t\bar{t}Z$ production (see e.g., [14]), they are at the moment subleading compared to residual uncertainties from scale variation.

Our POWHEG BOX implementations provide event files in the LHA format [54] that we subsequently process with PYTHIA8.240 [55] using the `Monash 2013` tune [56]. For our simulations we deactivate multiparton interactions (MPI) and hadronization effects and switch off QED showering.

If not specified otherwise, in our phenomenological analyses cuts are imposed on the transverse momentum and pseudorapidity of the electron and positron of the $t\bar{t}e^+e^-$ final state,

$$p_T^e > 10 \text{ GeV}, \qquad |\eta^e| < 2.5, \tag{7}$$

and on the invariant mass of the e^+e^- system, restricting it to a window around the Z-boson mass, i.e.:

$$m_Z - 10\ \text{GeV} \leq M_{e^+e^-} \leq m_Z + 10\ \text{GeV}. \tag{8}$$

When decays of the top and antitop quarks are taken into account, namely $t \to \mu^+\nu_\mu b$ and $\bar{t} \to \mu^-\bar{\nu}_\mu \bar{b}$, the following additional cuts on the muons' transverse momenta and pseudorapidity are also imposed,

$$p_T^\mu > 10\ \text{GeV}, \qquad |\eta^\mu| < 2.5. \tag{9}$$

A. Features of the NLO QCD corrections to $t\bar{t}\ell^+\ell^-$ production

In order to assess the theoretical uncertainty of our fixed-order predictions, we consider total and differential cross sections for $pp \to t\bar{t}e^+e^-$ after the lepton cuts of Eqs. (7) and (8) have been applied and investigate the impact of NLO QCD corrections and their dependence on the renormalization and factorization scales. First of all we notice that total cross sections show a very mild dependence on the nature of the renormalization and factorization scales. Choosing the fixed scale of Eq. (4) we obtain the following LO and NLO QCD cross sections:

$$\begin{aligned} \sigma^{\text{LO}}_{t\bar{t}e^+e^-} &= 15.9^{+5.1}_{-3.6}\ \text{fb}, \\ \sigma^{\text{NLO}}_{t\bar{t}e^+e^-} &= 21.9^{+2.0}_{-2.4}\ \text{fb}, \end{aligned} \tag{10}$$

while the corresponding results when using the dynamical scale of Eq. (5) are

$$\begin{aligned} \sigma^{\text{LO}}_{t\bar{t}e^+e^-} &= 15.8^{+5.0}_{-3.5}\ \text{fb}, \\ \sigma^{\text{NLO}}_{t\bar{t}e^+e^-} &= 22.1^{+2.2}_{-2.5}\ \text{fb}, \end{aligned} \tag{11}$$

where LO and NLO QCD results have been calculated for the same choice of NLO PDF and α_s while the quoted uncertainties are from renormalization and factorization scale variation, as discussed in the beginning of Sec. III.

Figures 2–5illustrate the differential distributions of a variety of observables built from the momenta of the top quarks at LO and NLO QCD. In each figure the upper panel shows LO and NLO QCD results for a given distribution using the fixed scale of Eq. (4) and the corresponding uncertainty band obtained from scale variation, while the middle and lower panels give the bin-by-bin ratios of NLO QCD versus LO results (i.e., the so-called differential K factor) obtained using the fixed and dynamical scale choices of Eqs. (4) and (5), respectively. In general, the middle and lower panels in Figs. 2–5show a very similar behavior when considering either a fixed or a dynamical scale, even at the differential level, and well summarize the impact and residual perturbative uncertainty on the theoretical prediction for $t\bar{t}\ell^+\ell^-$ production including NLO QCD corrections.

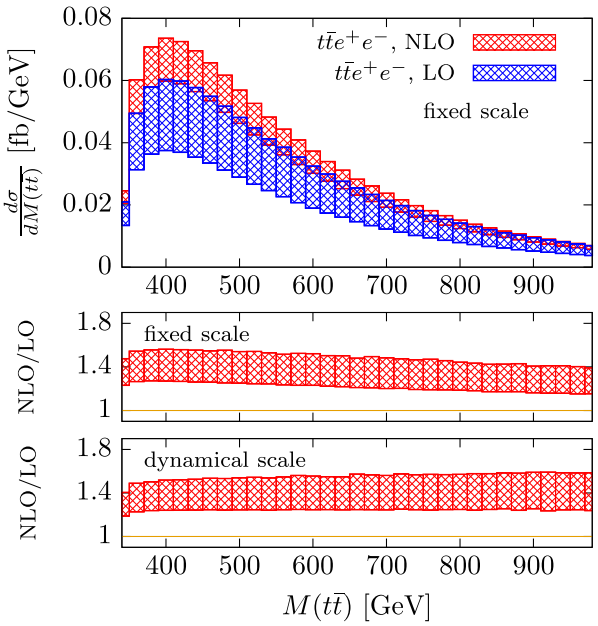

FIG. 2. Invariant mass distribution of the $t\bar{t}$ pair in $t\bar{t}e^+e^-$ production at LO (blue) and NLO QCD (red) accuracy.

More specifically, in Fig. 2 we see that the NLO QCD corrections to the invariant mass distribution of the $t\bar{t}$ system ($M(t\bar{t})$) are quite large and uniformly affect the corresponding LO results over the extended range considered in Fig. 2. On the other hand, as illustrated by Fig. 3, the transverse momentum distribution of the $t\bar{t}$ system ($p_T(t\bar{t})$) receives larger NLO QCD corrections in the high-p_T regime, where the scale uncertainty is also larger. A similar behavior has been previously observed in calculations of $t\bar{t}W^\pm$ production [25]. In contrast, the p_T distribution of the top quark ($p_T(t)$) receives larger NLO QCD corrections in the low p_T region. Both the variation of the relative NLO QCD correction and of its scale uncertainty throughout the shown transverse momentum range are less pronounced for the top quark than for the $t\bar{t}$ system. The case of $p_T(t\bar{t})$ and $p_T(t)$ distributions is also the only case in which we notice a mild difference between using a fixed and a dynamical renormalization and factorization scale. Using a dynamical scale seems to enhance the effect of NLO QCD corrections in the high-$p_T(t\bar{t})$ region, while it gives a more uniform K factor in the case of the $p_T(t)$ distribution.

For the top-quark rapidity ($y(t)$) and the rapidity difference of top quark and antiquark ($\Delta y(t,\bar{t})$), shown in Fig. 4, the relative NLO QCD corrections become larger for higher values of $y(t)$ and $\Delta y(t,\bar{t})$, and the associated scale uncertainties also increase with the absolute value of the rapidity or rapidity difference. Figure 5 shows the distribution of the azimuthal-angle difference ($\Delta\Phi(t,\bar{t})$) between the momenta of the top quark and antiquark. We observe larger relative NLO QCD corrections and larger scale

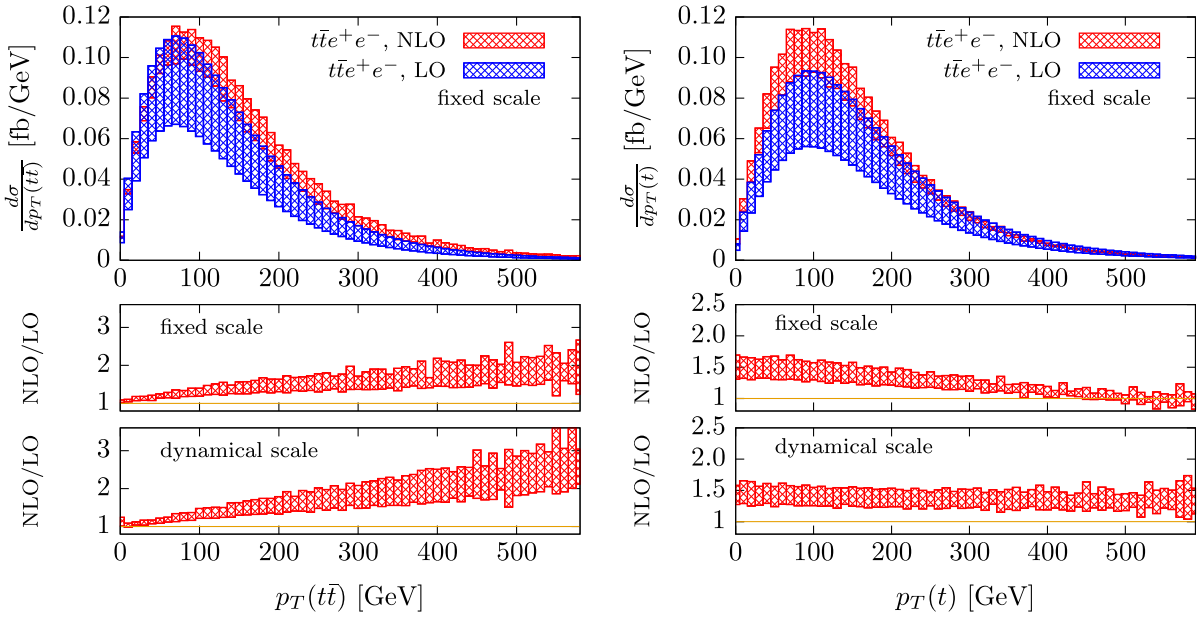

FIG. 3. Transverse-momentum distribution of the $t\bar{t}$ system (left) and of the top quark (right) obtained with our $t\bar{t}e^+e^-$ implementations at LO (blue) and NLO QCD (red) accuracy.

uncertainties for both scale choices in the low $\Delta\phi(t\bar{t})$ region than at high values of $\Delta\phi(t\bar{t})$.

Finally, we consider the charge asymmetry of the $t\bar{t}$ system. In processes involving top-quark pairs, charge asymmetries of the $t\bar{t}$ system or its decay products have received considerable attention (see, e.g., Ref. [23] for the case of $t\bar{t}W$ production) for constraining effects of physics beyond the SM. In particular, the charge asymmetry A_c is sensitive to differences in the absolute values of the rapidity distributions of the top quark and antiquark,

$$\Delta y_{t\bar{t}} = |y_t| - |y_{\bar{t}}|. \tag{12}$$

With $\sigma(\Delta y_{t\bar{t}} > 0)$ $[\sigma(\Delta y_{t\bar{t}} < 0)]$ denoting the part of the full cross section within a given set of cuts with positive [negative] values of $\Delta y_{t\bar{t}}$, this charge asymmetry is defined as

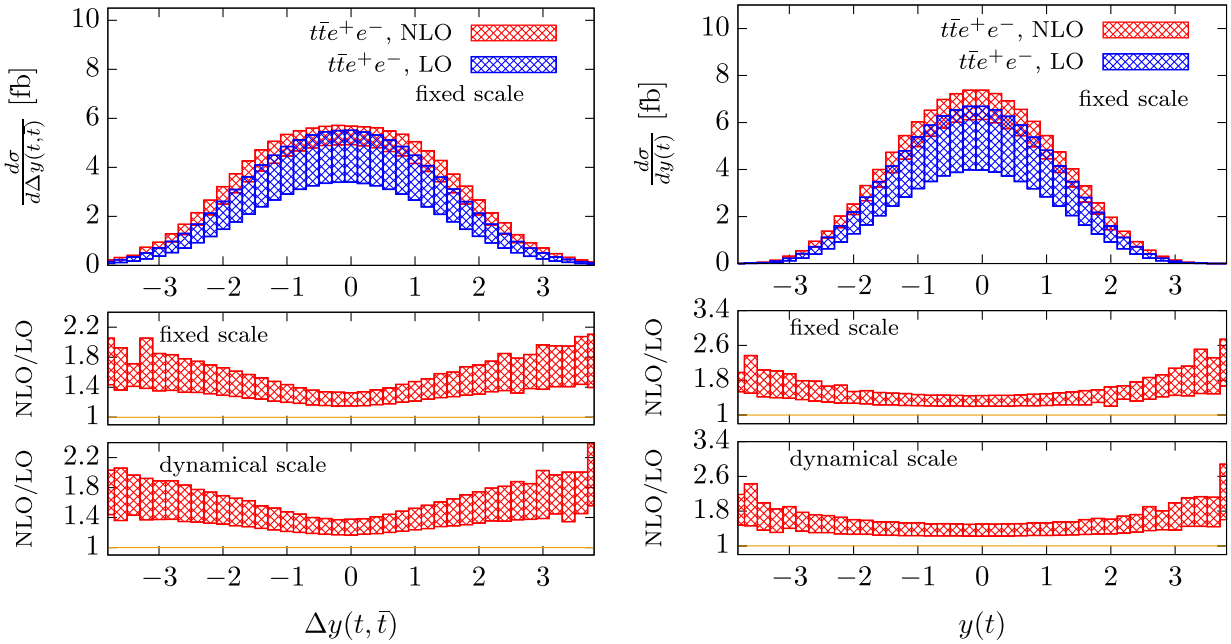

FIG. 4. Distribution of the rapidity separation of the top and antitop quark (left) and of the top quark (right) obtained with our $t\bar{t}e^+e^-$ implementation at LO and NLO QCD accuracy.

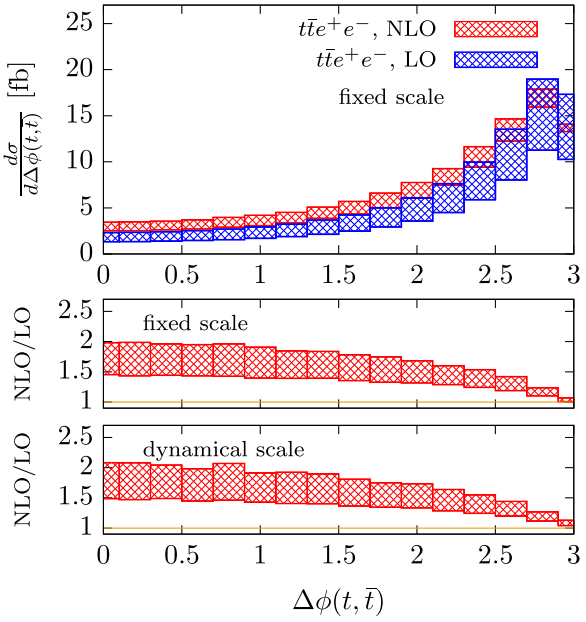

FIG. 5. Distribution of the azimuthal angle separation of the top from the antitop obtained with our $t\bar{t}e^+e^-$ implementations at LO and NLO QCD accuracy.

$$A_c = \frac{\sigma(\Delta y_{t\bar{t}} > 0) - \sigma(\Delta y_{t\bar{t}} < 0)}{\sigma(\Delta y_{t\bar{t}} > 0) + \sigma(\Delta y_{t\bar{t}} < 0)}, \tag{13}$$

where the cross section for each term in the numerator and denominator is evaluated at NLO QCD accuracy. While each of the entries in this quantity can be sizable, large cancellations between cross-section contributions with rapidity differences of opposite sign result in rather small values of A_c, which makes the numerical calculation of the asymmetry challenging. We note that a similar trend in the simulation of the charge asymmetry was reported in the context of $t\bar{t}$ and $t\bar{t}+$jet production at the LHC in Ref. [57] and Ref. [49], respectively. As discussed in Ref. [57], for instance, the definition of A_c of Eq. (13) introduces contributions beyond NLO QCD which are not under control. This can be avoided by expanding A_c consistently up to $\mathcal{O}(\alpha_s)$ which yields

$$A_c^{ex} = A_c \frac{\sigma^{\rm NLO}_{t\bar{t}e^+e^-}}{\sigma^{\rm LO}_{t\bar{t}e^+e^-}}, \tag{14}$$

with the unexpanded charge asymmetry A_c of Eq. (13) and the inclusive $t\bar{t}e^+e^-$ cross section at NLO QCD ($\sigma^{\rm NLO}_{t\bar{t}e^+e^-}$) and LO ($\sigma^{\rm LO}_{t\bar{t}e^+e^-}$) accuracy. For the unexpanded charge asymmetry of Eq. (13) and the expanded charge asymmetry of Eq. (14) in $t\bar{t}e^+e^-$ production, we find using the fixed scale of Eq. (4):

$$A_c = 0.84^{+0.28}_{-0.19}\%, \qquad A_c^{ex} = 1.15^{+0.11}_{-0.18}\%, \tag{15}$$

and for the dynamical scale of Eq. (5):

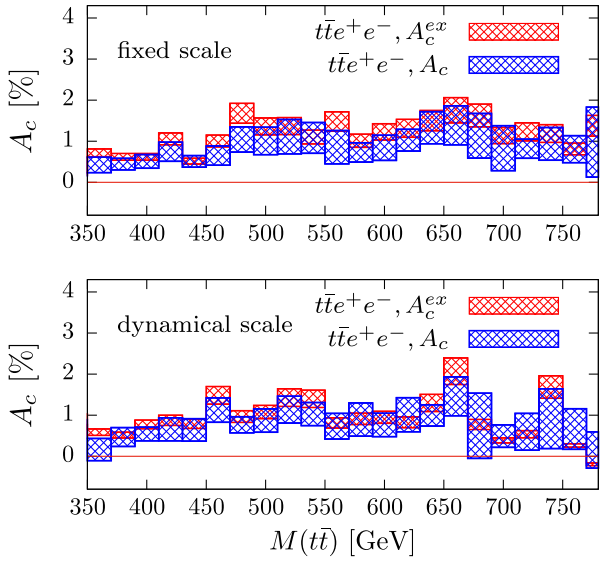

FIG. 6. The expanded charge asymmetry $A_c^{ex}(M_{t\bar{t}})$ (red) and unexpanded charge asymmetry $A_c(M_{t\bar{t}})$ (blue) for the fixed (top) and dynamical scale (bottom) choice as functions of the invariant mass of the $t\bar{t}$ pair in $t\bar{t}e^+e^-$ production.

$$A_c = 0.74^{+0.25}_{-0.18}\%, \qquad A_c^{ex} = 1.04^{+0.20}_{-0.17}\%. \tag{16}$$

As illustrated by Fig. 6, where the charge asymmetry is shown as a function of the invariant mass of the $t\bar{t}$ system, the scale uncertainty is smaller for A_c^{ex} than for A_c for both the fixed and dynamical scale choices. This is expected due to the consistent matching of perturbative orders in the expanded expressions for the asymmetry. We therefore recommend to use the expanded charge asymmetry when comparing with a measurement of A_c even though the unexpanded and expanded charge asymmetries are compatible within their respective scale uncertainties.

B. Assessment of off-shell effects in the $\ell^+\ell^-$ system

After having established the main theoretical uncertainty of NLO QCD predictions for $t\bar{t}\ell^+\ell^-$ production, we explore the sensitivity of $t\bar{t}\ell^+\ell^-$ results to off-shell and lepton spin-correlation effects through a comparison of $t\bar{t}e^+e^-$ with $t\bar{t}Z$ on-shell production matched, in the narrow-width approximation, to $Z \to e^+e^-$ via the PYTHIA decay feature. We consider observables involving the momenta of the Z boson's decay leptons and compare results obtained from our $t\bar{t}e^+e^-$ and $t\bar{t}Z$ implementations. In both cases top and antitop quark's decays ($t \to \mu^+\nu_\mu b$ and $\bar{t} \to \mu^-\bar{\nu}_\mu \bar{b}$) are treated using the decay feature of PYTHIA, since we first aim at isolating effects arising only from spin-correlations and off-shellness of the leptons not coming from top-quark decays.

The $t\bar{t}e^+e^-$ implementation fully accounts for off-shell contributions and spin correlations in diagrams where a Z boson decays into an e^+e^- pair, and also includes diagrams

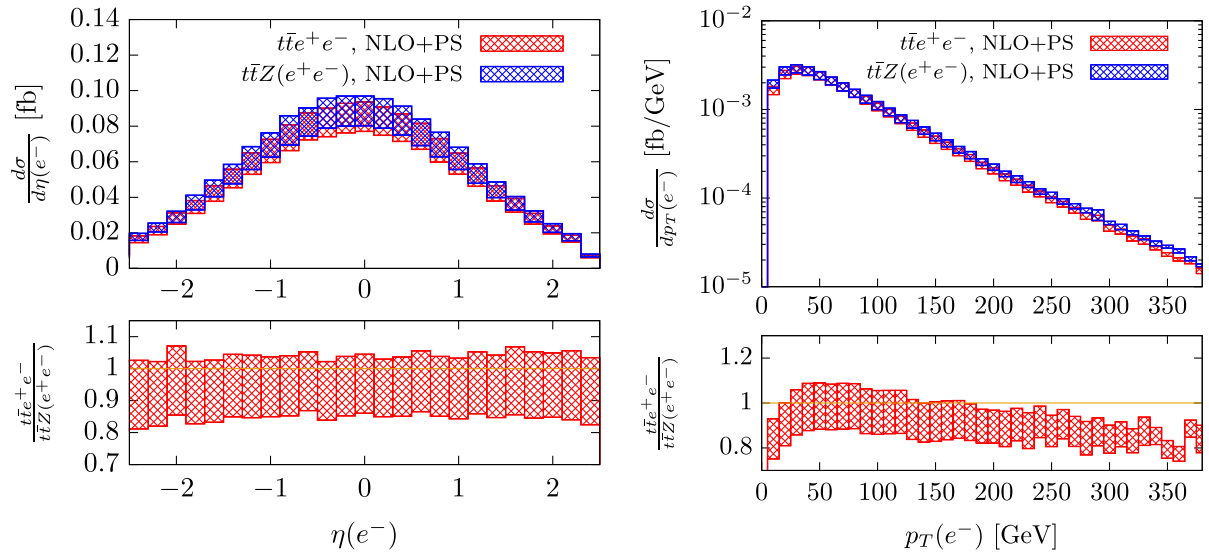

FIG. 7. Pseudorapidity (left) and transverse-momentum distribution (right) of the electron obtained with our $t\bar{t}Z$ (blue) and $t\bar{t}e^+e^-$ (red) implementations, respectively, at NLO + PS accuracy.

where the lepton pair stems from a photon rather than a Z boson. While the e^+e^- final-state system is described with full NLO QCD accuracy in our $t\bar{t}e^+e^-$ implementation, in the $t\bar{t}Z$ program decay products of the Z boson can only be accounted for when event files providing momenta for the $t\bar{t}Z$ system are processed with a multipurpose Monte-Carlo event generator like PYTHIA, capable to simulate decays of on-shell particles with no spin-correlation effects at LO accuracy. Such an approach does not capture off-shell effects or spin correlations in the decay and, moreover, entirely neglects contributions to the $t\bar{t}e^+e^-$ final state due to diagrams where a photon is exchanged rather than a Z boson. A detailed comparison of observables that might be particularly sensitive to such effects reveals that the two implementations differ in specific regions of phase space, as illustrated in Figs. 7–9. It is interesting to notice that such effects are visible even if we restrict the fiducial volume to a window region around the mass of the Z boson by using the cut of Eq. (8). Since the features observed in Figs. 7–9 could be due to both off-shell effects and spin-correlation effects, we have then tried to establish their main origin by studying the dependence on the cut imposed on $M_{e^+e^-}$. We noticed that such features very mildly depend on requiring that $M_{e^+e^-} \geq M^{\min}_{e^+e^-}$ when $M^{\min}_{e^+e^-}$ is varied from 10 to 80 GeV at the analysis level, while keeping the corresponding generation cut on $M_{e^+e^-}$ at 1, 5, or 10 GeV. We interpret

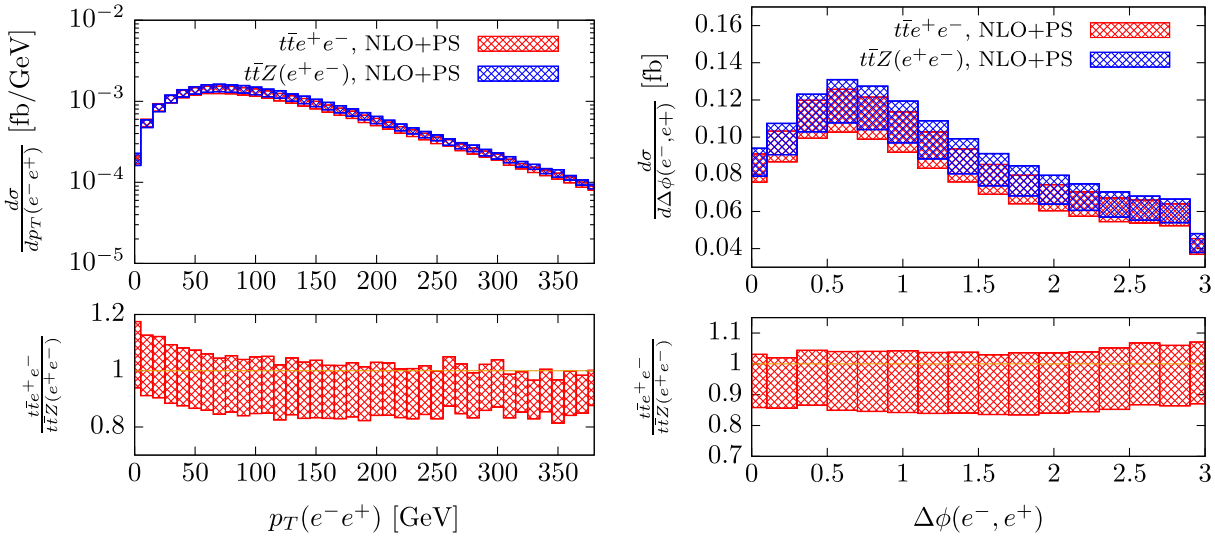

FIG. 8. Transverse-momentum distribution of the e^+e^- system (left) and azimuthal angle separation of the electron from the positron (right) obtained with our $t\bar{t}Z$ (blue) and $t\bar{t}e^+e^-$ (red) implementations, respectively, at NLO + PS accuracy.

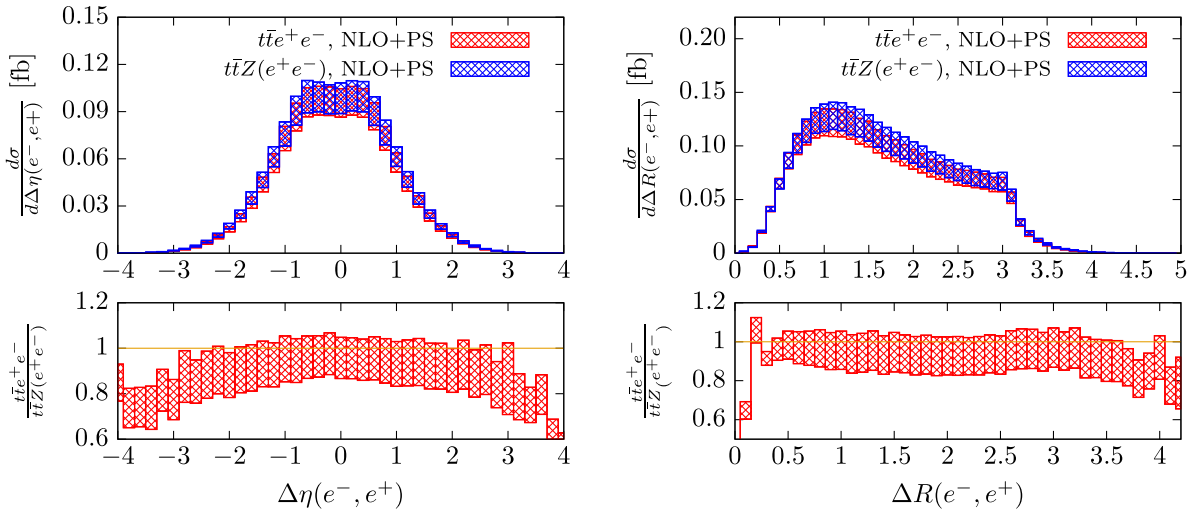

FIG. 9. Distribution of the pseudorapidity separation (left) and ΔR separation of the electron from the positron (right) obtained with our $t\bar{t}Z$ (blue) and $t\bar{t}e^+e^-$ (red) implementations, respectively, at NLO + PS accuracy.

this as an indication that the features seen in Figs. 7–9 are mainly due to spin-correlation effects.

The following discussion is based on NLO + PS results obtained with PYTHIA. The electron cuts of Eqs. (7) and (8) are applied. The corresponding total cross sections including scale uncertainties for the fixed scale choice of Eq. (4) are

$$\sigma^{\mathrm{NLO+PS}}_{t\bar{t}Z(e^+e^-)} = 0.274^{+0.025}_{-0.030}\ \mathrm{fb},$$
$$\sigma^{\mathrm{NLO+PS}}_{t\bar{t}e^+e^-} = 0.261^{+0.024}_{-0.028}\ \mathrm{fb}, \tag{17}$$

and for the dynamical scale of Eq. (5) we find

$$\sigma^{\mathrm{NLO+PS}}_{t\bar{t}Z(e^+e^-)} = 0.275^{+0.028}_{-0.031}\ \mathrm{fb},$$
$$\sigma^{\mathrm{NLO+PS}}_{t\bar{t}e^+e^-} = 0.264^{+0.027}_{-0.030}\ \mathrm{fb}. \tag{18}$$

We present results for the pseudorapidity ($\eta(e^-)$) and transverse-momentum ($p_T(e^-)$) distributions of the electron in Fig. 7, the transverse-momentum ($p_T(e^-e^+)$) and azimuthal-angle separation ($\Delta\phi(e^-,e^+)$) of the e^+e^- system in Fig. 8, as well as its pseudorapidity separation ($\Delta\eta(e^-,e^+)$) and ΔR separation ($\Delta R(e^-,e^+)$) in Fig. 9, where $\Delta R(\ell^-,\ell^+)$ is defined in terms of $\Delta\phi$ and $\Delta\eta$ of a generic $\ell^-\ell^+$ pair as:

$$\Delta R(\ell^-,\ell^+) = \sqrt{\Delta\phi^2(\ell^-,\ell^+) + \Delta\eta^2(\ell^-,\ell^+)}. \tag{19}$$

The differential distributions obtained with our $t\bar{t}e^+e^-$ and $t\bar{t}Z$ implementations and shown in Figs. 7–9agree within the scale uncertainty band in most regions of phase space. However, there are substantial effects of the order of 10%–20%, visible outside the scale uncertainty band, most notably in the high-p_T region of the electron/positron transverse-momentum distribution as illustrated in Fig. 7 for the case of $p_T(e^-)$, in the large absolute-value region of the pseudorapidity difference $\Delta\eta(e^-,e^+)$ and in corresponding regions of the $\Delta R(e^-,e^+)$ distance as one can see in Fig. 9.

C. Assessment of spin correlations in top decays

Next, we would like to assess the effect of modeling on-shell top-quark decays, in the narrow-width approximation, including tree-level spin correlations as obtained in our $t\bar{t}e^+e^-$ implementation following the method of Ref. [37] versus a more approximate treatment where decays of the top quarks are simulated by the decay feature of PYTHIA and no spin correlations are retained. For simplicity, in the following these two simulations are referred to as *with spin correlations* and *without spin correlations*, although in both cases spin correlations in the e^+e^- system are fully taken into account. We remind the reader that, as explained in Sec. II, both options are available in our POWHEG BOX implementation. In the first case, at the Les-Houches event (LHE) level before parton shower, the program generates fully decayed events, i.e., $(t \to \mu^+\nu_\mu b)(\bar{t} \to \mu^-\bar{\nu}_\mu\bar{b})e^+e^-$, while in the second case only $t\bar{t}e^+e^-$ events are generated.

For the results shown in this section, the muon cuts of Eq. (9) are applied in addition to the electron cuts of Eqs. (7) and (8). The corresponding total cross sections including scale uncertainties for the fixed scale choice of Eq. (4) are

$$\text{with spin corr:}\ \sigma^{\mathrm{NLO+PS}}_{t\bar{t}e^+e^-} = 0.199^{+0.030}_{-0.011}\ \mathrm{fb},$$
$$\text{w/o spin corr:}\ \sigma^{\mathrm{NLO+PS}}_{t\bar{t}e^+e^-} = 0.214^{+0.019}_{-0.023}\ \mathrm{fb}, \tag{20}$$

while for the dynamical scale of Eq. (5) we find

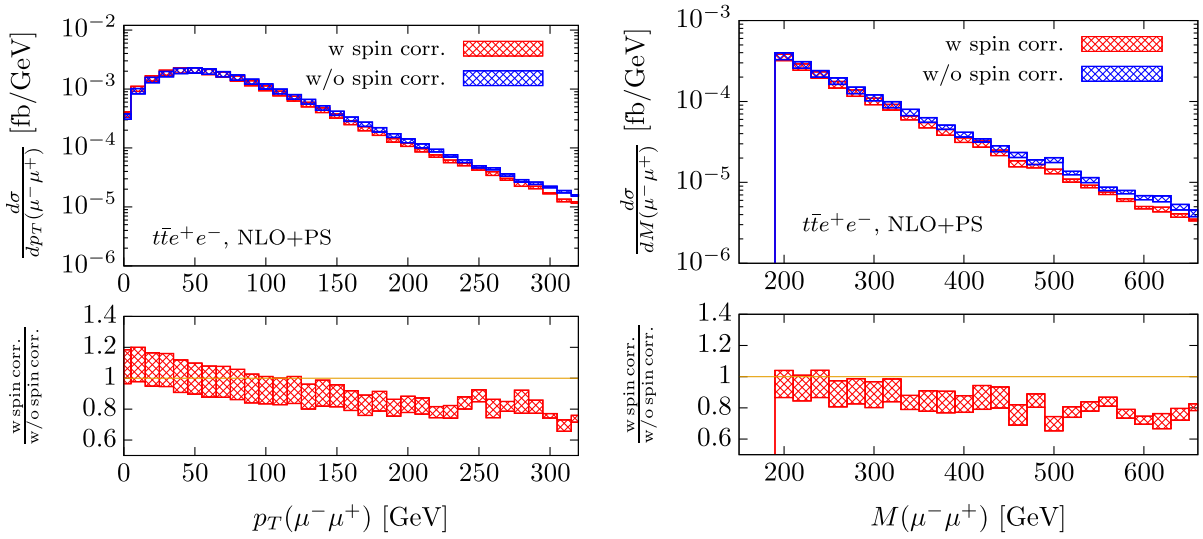

FIG. 10. Transverse-momentum (left) and invariant-mass distribution of the $\mu^+\mu^-$ system (right) in the $pp \to (t \to \mu^+\nu_\mu b)(\bar{t} \to \mu^-\bar{\nu}_\mu \bar{b})e^+e^-$ process at NLO + PS accuracy. Correlations in the top-quark decays are either taken into account at the level of event generation (red) or provided by PYTHIA (blue).

$$\text{with spin corr: } \sigma^{\text{NLO+PS}}_{t\bar{t}e^+e^-} = 0.216^{+0.021}_{-0.024} \text{ fb},$$
$$\text{w/o spin corr: } \sigma^{\text{NLO+PS}}_{t\bar{t}e^+e^-} = 0.213^{+0.020}_{-0.023} \text{ fb}. \quad (21)$$

As expected, effects on the total cross section are small (in fact the cross sections are compatible within the scale uncertainties), while they are more relevant in specific regions of kinematic distributions. Indeed, a more detailed comparison of the two approaches in terms of distributions of kinematic observables built from the momenta of the top-quark and Z-boson decay products reveals the presence of non-negligible effects, in particular for observables of the $(\mu^+\mu^-)$ system.

A clear example is illustrated in Fig. 10, where we show the transverse momentum $(p_T(\mu^-\mu^+))$ and the invariant mass $(M(\mu^-\mu^+))$ distributions of the $\mu^+\mu^-$ system. The tails of both of these distributions are considerably lower, by roughly 10%–20%, for the predictions that take into account spin correlations in the top-quark decays and the effect is clearly visible on top of the renormalization and factorization scale uncertainty considered in our study. A similar effect can be observed in the transverse-momentum distribution of the muons $(p_T(\mu^\pm))$, as depicted in Fig. 11

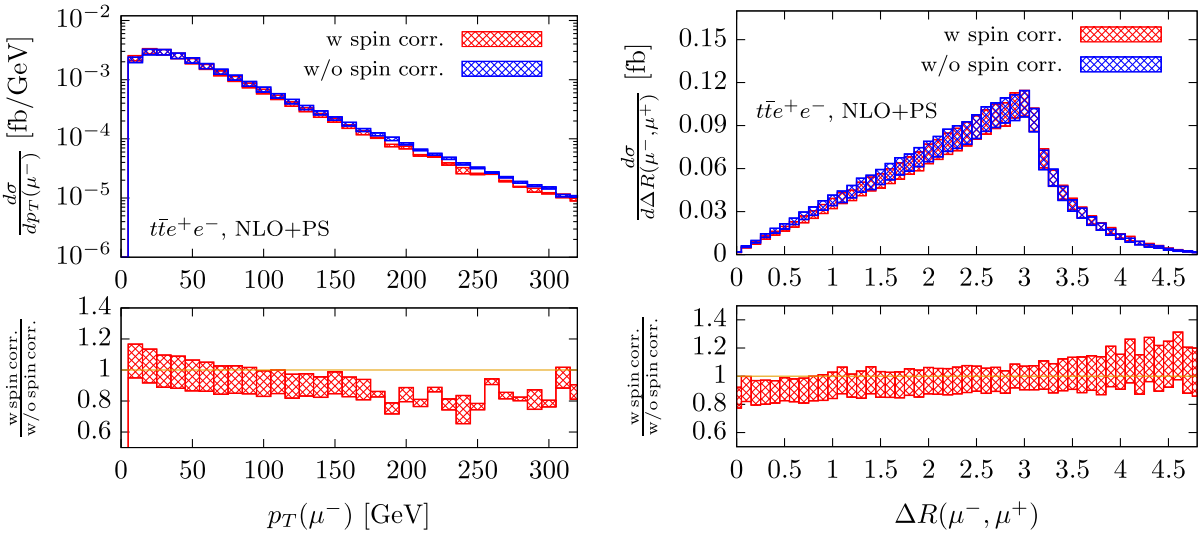

FIG. 11. Transverse-momentum distribution of the muon (left) and ΔR separation of the μ^- from the μ^+ (right) in the $pp \to (t \to \mu^+\nu_\mu b)(\bar{t} \to \mu^-\bar{\nu}_\mu \bar{b})e^+e^-$ process at NLO + PS accuracy. Correlations in the top-quark decays are either taken into account at the level of event generation (red) or provided by PYTHIA (blue).

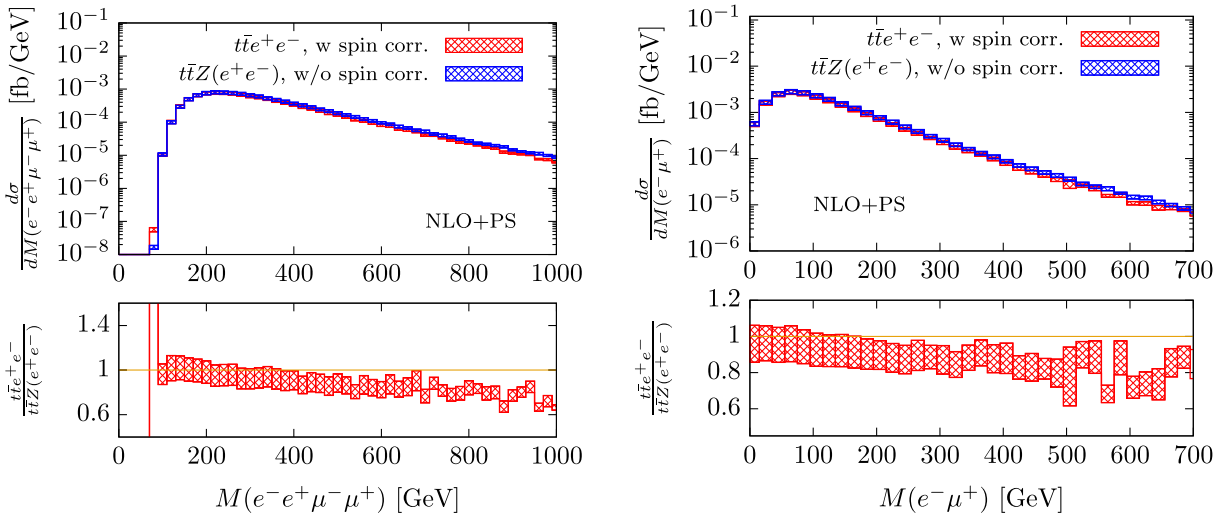

FIG. 12. Invariant-mass distribution of the $e^+e^-\mu^+\mu^-$ system (left) and of the $e^-\mu^+$ system (right) in the $pp \to (t \to \mu^+\nu_\mu b)(\bar{t} \to \mu^-\bar{\nu}_\mu \bar{b})e^+e^-$ and $pp \to (t \to \mu^+\nu_\mu b)(\bar{t} \to \mu^-\bar{\nu}_\mu \bar{b})(Z \to e^+e^-)$ processes at NLO + PS accuracy. Correlations in the top-quark and Z-boson decays are either taken into account at the level of event generation (red) or provided by PYTHIA (blue).

for the case of $p_T(\mu^-)$. Milder yet visible effects are observed in angular distributions such as the ΔR separation of μ^- from μ^+ defined as in Eq. (19), which is dominated by contributions of low or moderate transverse momentum.

Having access to the momenta of the muons stemming from the top-quark decays as well as to the e^+e^- system, we can also explore correlations between the various final-state leptons in the $pp \to (t \to \mu^+\nu_\mu b)(\bar{t} \to \mu^-\bar{\nu}_\mu \bar{b})e^+e^-$ process. As an example, we present in Fig. 12 the invariant mass distributions of the $e^+e^-\mu^+\mu^-$ and the $e^-\mu^+$ systems, respectively, and we compare results obtained using the $t\bar{t}e^+e^-$ implementation with spin-correlated top decays versus those obtained from the corresponding implementation of $t\bar{t}Z$ with on-shell $Z \to e^+e^-$ decays via PYTHIA default routines, i.e., without spin correlations. Both distributions show 10%–20% off-shell and spin-correlation effects for high invariant masses, while we do not find appreciable effects in the case of angular distributions of the $e^\pm\mu^\mp$ systems, such as pseudorapidity differences and ΔR separations, as illustrated in Fig. 13 for the $e^-\mu^+$ case.

IV. SUMMARY AND CONCLUSIONS

In this article we present results for the production of $t\bar{t}\ell^+\ell^-$ at the LHC with $\sqrt{s} = 13$ TeV including NLO

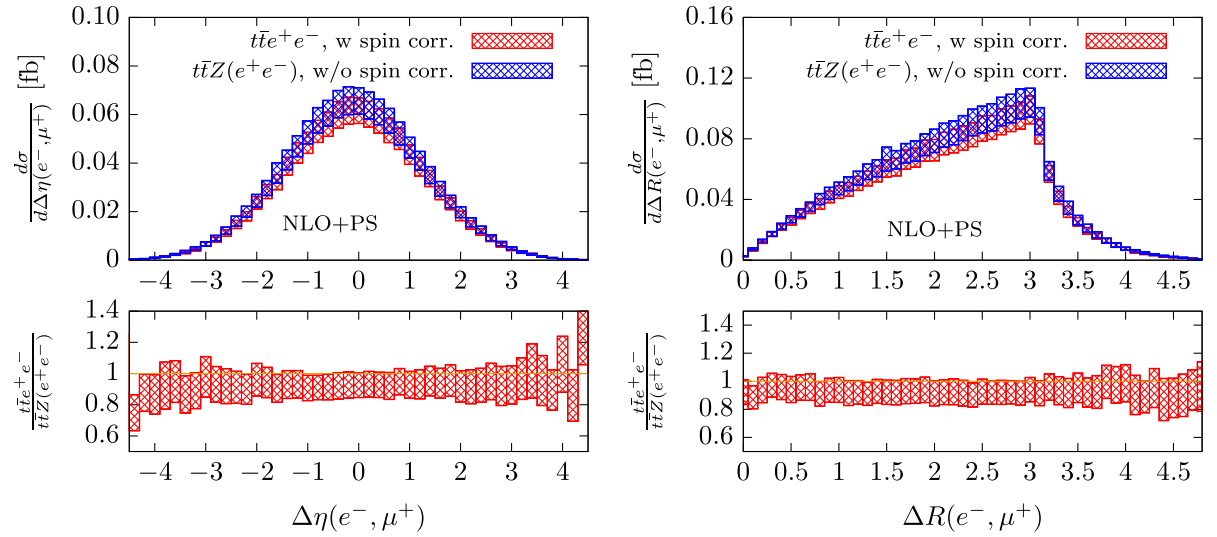

FIG. 13. Distribution of the pseudorapidity separation (left) and ΔR separation of the electron from the μ^+ (right) in the $pp \to (t \to \mu^+\nu_\mu b)(\bar{t} \to \mu^-\bar{\nu}_\mu \bar{b})e^+e^-$ and $pp \to (t \to \mu^+\nu_\mu b)(\bar{t} \to \mu^-\bar{\nu}_\mu \bar{b})(Z \to e^+e^-)$ processes at NLO + PS accuracy. Correlations in the top-quark and Z-boson decays are either taken into account at the level of event generation (red) or provided by PYTHIA (blue).

QCD corrections matched to parton showers via the POWHEG method. The option for simulating decays of the top quarks in a narrow-width approximation including tree-level spin correlations is provided.

We explicitly study the impact of off-shell effects by comparing results for $t\bar{t}\ell^+\ell^-$ production versus results obtained from $t\bar{t}Z$ on-shell production matched to the $Z \to \ell^+\ell^-$ decay in a narrow-width approximation. For illustration purposes we specify our discussion to the $t\bar{t}e^+e^-$ case. We find general compatibility between the two implementations, but we also notice sizable effects at the 10%–20% level, clearly visible in the tails of the leptons' transverse-momentum distributions, as well as in the transverse momentum and pseudorapity distributions of the $\ell^+\ell^-$ system.

Furthermore, we investigate the effect of considering approximate spin-correlations among the leptons from top quark and antiquark decays, as well as among all leptons in the final-state signatures (from both Z-boson and top/antitop decays). We illustrate our results for the specific case of $t\bar{t}e^+e^-$ with $t \to \mu^+\nu_\mu b$ and $\bar{t} \to \mu^-\bar{\nu}_\mu\bar{b}$. Although small at the level of total cross sections, these effects can reach 10%–20% in tails of distributions for transverse momenta and invariant masses of the Z-boson and the top-quark and top-antiquark decay products.

Our implementations of $t\bar{t}\ell^+\ell^-$ and $t\bar{t}Z$ in POWHEG BOX allow to study any other $t\bar{t}\ell^+\ell^-$ signature, provided due care is taken to adjust the selection of the desired final state signature. Hence, our study and the tools developed in its context represent substantial progress toward a full description of production and decay of a $t\bar{t}\ell^+\ell^-$ system at hadron colliders, including NLO QCD corrections matched with parton shower, and will allow a more adequate assessment of the theoretical uncertainty stemming from the modeling of the kind of complex final states that are considered in LHC measurements of SM properties and searches of new physics. In particular they will allow a more accurate exploration of the properties of the top quark and its interactions with EW gauge bosons and the Higgs boson, where the $t\bar{t}Z$ signatures play a major role either as signal or background, respectively. With this respect, the kind of effects described in this paper can be of great relevance since new physics effects tend to appear in high-mass and high-momentum tails of distributions that will become more and more statistically significant with the upcoming high-luminosity runs of the LHC.

Both the $t\bar{t}\ell^+\ell^-$ and $t\bar{t}Z$ implementations that we developed for this study will be made available from the website of the POWHEG BOX project, [58].

ACKNOWLEDGMENTS

The authors would like to thank M. Kraus and C. Oleari for valuable discussions and help with several aspects of the POWHEG BOX implementation. M. G., B. J., and S. L. would like to thank J. Scheller and C. Borschensky for helpful conversations. L. R. would like to thank D. Figueroa and S. Quackenbush for their support in optimizing the use of NLOX for this project. The work of L. R. is supported in part by the U.S. Department of Energy under Grant No. DE-SC0010102. The work of D. W. is supported in part by the U.S. National Science Foundation under Grants No. PHY-1719690 and No. PHY-2014021. Part of this work was performed on the high-performance computing resource bwForCluster NEMO with support by the state of Baden-Württemberg through bwHPC and the German Research Foundation (DFG) through Grant No. INST 39/963-1 FUGG.

[1] M. Aaboud *et al.* (ATLAS Collaboration), Measurement of the $t\bar{t}Z$ and $t\bar{t}W$ production cross sections in multilepton final states using 3.2 fb^{-1} of pp collisions at $\sqrt{s} =$ 13 TeV with the ATLAS detector, Eur. Phys. J. C **77,** 40 (2017).

[2] M. Aaboud *et al.* (ATLAS Collaboration), Measurement of the $t\bar{t}Z$ and $t\bar{t}W$ cross sections in proton-proton collisions at $\sqrt{s} = 13$ TeV with the ATLAS detector, Phys. Rev. D **99,** 072009 (2019).

[3] G. Aad *et al.* (ATLAS Collaboration), Measurements of the inclusive and differential production cross sections of a top-quark-antiquark pair in association with a Z boson at $\sqrt{s} = 13$ TeV with the ATLAS detector, Eur. Phys. J. C **81,** 737 (2021).

[4] A. M. Sirunyan *et al.* (CMS Collaboration), Measurement of the cross section for top quark pair production in association with a W or Z boson in proton-proton collisions at $\sqrt{s} = 13$ TeV, J. High Energy Phys. 08 (2018) 011.

[5] CMS Collaboration, Measurement of top quark pair production in association with a Z boson in proton-proton collisions at $\sqrt{s} = 13$ TeV, Report No. CMS-PAS-TOP-18-009, 2019.

[6] J. M. Campbell and R. K. Ellis, $t\bar{t}W^\pm$ production and decay at NLO, J. High Energy Phys. 07 (2012) 052.

[7] M. V. Garzelli, A. Kardos, C. G. Papadopoulos, and Z. Trocsanyi, $t\bar{t}W^\pm$ and $t\bar{t}Z$ hadroproduction at NLO accuracy in QCD with parton shower and hadronization effects, J. High Energy Phys. 11 (2012) 056.

[8] F. Maltoni, D. Pagani, and I. Tsinikos, Associated production of a top-quark pair with vector bosons at NLO in QCD: Impact on $t\bar{t}H$ searches at the LHC, J. High Energy Phys. 02 (2016) 113.

[9] S. Frixione, V. Hirschi, D. Pagani, H. S. Shao, and M. Zaro, Electroweak and QCD corrections to top-pair hadroproduction in association with heavy bosons, J. High Energy Phys. 06 (2015) 184.

[10] R. Frederix, D. Pagani, and M. Zaro, Large NLO corrections in $t\bar{t}W^{\pm}$ and $t\bar{t}t\bar{t}$ hadroproduction from supposedly subleading EW contributions, J. High Energy Phys. 02 (2018) 031.

[11] R. Frederix and I. Tsinikos, Subleading EW corrections and spin-correlation effects in $t\bar{t}W$ multi-lepton signatures, Eur. Phys. J. C **80**, 803 (2020).

[12] A. Lazopoulos, T. McElmurry, K. Melnikov, and F. Petriello, Next-to-leading order QCD corrections to $t\bar{t}Z$ production at the LHC, Phys. Lett. B **666**, 62 (2008).

[13] A. Kardos, Z. Trocsanyi, and C. Papadopoulos, Top quark pair production in association with a Z-boson at NLO accuracy, Phys. Rev. D **85**, 054015 (2012).

[14] D. de Florian *et al.* (LHC Higgs Cross Section Working Group Collaboration), Handbook of LHC Higgs cross sections: 4. Deciphering the nature of the Higgs sector, Report No. CERN-2017-002-M, 2017.

[15] H. T. Li, C. S. Li, and S. A. Li, Renormalization group improved predictions for $t\bar{t}W^{\pm}$ production at hadron colliders, Phys. Rev. D **90**, 094009 (2014).

[16] A. Broggio, A. Ferroglia, G. Ossola, and B. D. Pecjak, Associated production of a top pair and a W boson at next-to-next-to-leading logarithmic accuracy, J. High Energy Phys. 09 (2016) 089.

[17] A. Broggio, A. Ferroglia, G. Ossola, B. D. Pecjak, and R. D. Sameshima, Associated production of a top pair and a Z boson at the LHC to NNLL accuracy, J. High Energy Phys. 04 (2017) 105.

[18] A. Kulesza, L. Motyka, D. Schwartländer, T. Stebel, and V. Theeuwes, Associated production of a top quark pair with a heavy electroweak gauge boson at NLO + NNLL accuracy, Eur. Phys. J. C **79**, 249 (2019).

[19] A. Broggio, A. Ferroglia, R. Frederix, D. Pagani, B. D. Pecjak, and I. Tsinikos, Top-quark pair hadroproduction in association with a heavy boson at NLO + NNLL including EW corrections, J. High Energy Phys. 08 (2019) 039.

[20] A. Kulesza, L. Motyka, D. Schwartländer, T. Stebel, and V. Theeuwes, Associated top quark pair production with a heavy boson: Differential cross sections at NLO + NNLL accuracy, Eur. Phys. J. C **80**, 428 (2020).

[21] S. von Buddenbrock, R. Ruiz, and B. Mellado, Anatomy of inclusive $t\bar{t}W$ production at hadron colliders, Phys. Lett. B **811**, 135964 (2020).

[22] M. V. Garzelli, A. Kardos, C. G. Papadopoulos, and Z. Trocsanyi, Z_0—boson production in association with a $t\bar{t}$ pair at NLO accuracy with parton shower effects, Phys. Rev. D **85**, 074022 (2012).

[23] F. Maltoni, M. L. Mangano, I. Tsinikos, and M. Zaro, Top-quark charge asymmetry and polarization in $t\bar{t}W^{\pm}$ production at the LHC, Phys. Lett. B **736**, 252 (2014).

[24] R. Frederix and I. Tsinikos, On improving NLO merging for $t\bar{t}W$ production, J. High Energy Phys. 11 (2021) 029.

[25] F. F. Cordero, M. Kraus, and L. Reina, Top-quark pair production in association with a $W^{\pm}$ gauge boson in the POWHEG-BOX, Phys. Rev. D **103**, 094014 (2021).

[26] P. Nason, A new method for combining NLO QCD with shower Monte Carlo algorithms, J. High Energy Phys. 11 (2004) 040.

[27] S. Frixione, P. Nason, and C. Oleari, Matching NLO QCD computations with parton shower simulations: The POWHEG method, J. High Energy Phys. 11 (2007) 070.

[28] S. Frixione and B. R. Webber, Matching NLO QCD computations and parton shower simulations, J. High Energy Phys. 06 (2002) 029.

[29] S. Frixione, P. Nason, and B. R. Webber, Matching NLO QCD and parton showers in heavy flavor production, J. High Energy Phys. 08 (2003) 007.

[30] G. Bevilacqua, H.-Y. Bi, H. B. Hartanto, M. Kraus, and M. Worek, The simplest of them all: $t\bar{t}W^{\pm}$ at NLO accuracy in QCD, J. High Energy Phys. 08 (2020) 043.

[31] G. Bevilacqua, H.-Y. Bi, H. B. Hartanto, M. Kraus, J. Nasufi, and M. Worek, NLO QCD corrections to off-shell $t\bar{t}W^{\pm}$ production at the LHC: Correlations and asymmetries, Eur. Phys. J. C **81**, 675 (2021).

[32] A. Denner and G. Pelliccioli, NLO QCD corrections to off-shell $t\bar{t}W^{+}$ production at the LHC, J. High Energy Phys. 11 (2020) 069.

[33] A. Denner and G. Pelliccioli, Combined NLO EW and QCD corrections to off-shell $t\bar{t}W$ production at the LHC, Eur. Phys. J. C **81**, 354 (2021).

[34] R. Röntsch and M. Schulze, Constraining couplings of top quarks to the Z boson in $t\bar{t} + Z$ production at the LHC, J. High Energy Phys. 07 (2014) 091.

[35] G. Bevilacqua, H. B. Hartanto, M. Kraus, T. Weber, and M. Worek, Towards constraining dark matter at the LHC: Higher order QCD predictions for $t\bar{t} + Z(Z \to \nu_{\ell}\bar{\nu}_{\ell})$, J. High Energy Phys. 11 (2019) 001.

[36] J. Hermann and M. Worek, The impact of top-quark modelling on the exclusion limits in $t\bar{t}$ + DM searches at the LHC, Eur. Phys. J. C **81**, 1029 (2021).

[37] S. Frixione, E. Laenen, P. Motylinski, and B. R. Webber, Angular correlations of lepton pairs from vector boson and top quark decays in Monte Carlo simulations, J. High Energy Phys. 04 (2007) 081.

[38] S. Alioli, P. Nason, C. Oleari, and E. Re, A general framework for implementing NLO calculations in shower Monte Carlo programs: The POWHEG BOX, J. High Energy Phys. 06 (2010) 043.

[39] H. B. Hartanto, B. Jäger, L. Reina, and D. Wackeroth, Higgs boson production in association with top quarks in the POWHEG BOX, Phys. Rev. D **91**, 094003 (2015).

[40] B. Jäger, L. Reina, and D. Wackeroth, Higgs boson production in association with b jets in the POWHEG BOX, Phys. Rev. D **93**, 014030 (2016).

[41] ATLAS Collaboration, Modelling of rare top quark processes at $\sqrt{s} = 13$ TeV in ATLAS, Technical Report No. ATL-PHYS-PUB-2020-024, CERN, Geneva, 2020.

[42] G. Bevilacqua, H. Y. Bi, F. Febres Cordero, H. B. Hartanto, M. Kraus, J. Nasufi, L. Reina, and M. Worek, Modeling uncertainties of $t\bar{t}W^{\pm}$ multilepton signatures, Phys. Rev. D **105**, 014018 (2022).

[43] S. Frixione, Z. Kunszt, and A. Signer, Three jet cross-sections to next-to-leading order, Nucl. Phys. **B467**, 399 (1996).

[44] J. Alwall, P. Demin, S. de Visscher, R. Frederix, M. Herquet, F. Maltoni, T. Plehn, D. L. Rainwater, and T. Stelzer, MadGraph/MadEvent v4: The new web generation, J. High Energy Phys. 09 (2007) 028.

[45] S. Honeywell, S. Quackenbush, L. Reina, and C. Reuschle, NLOX, a one-loop provider for standard model processes, Comput. Phys. Commun. **257**, 107284 (2020).

[46] D. Figueroa, S. Quackenbush, L. Reina, and C. Reuschle, Updates to the one-loop provider NLOX, Comput. Phys. Commun. **270**, 108150 (2022).

[47] A. Denner, S. Dittmaier, M. Roth, and D. Wackeroth, Predictions for all processes $e^+e^- \to$ fermions $+ \gamma$, Nucl. Phys. **B560**, 33 (1999).

[48] A. Denner, S. Dittmaier, M. Roth, and L. H. Wieders, Electroweak corrections to charged-current $e^+e^- \to 4$ fermion processes: Technical details and further results, Nucl. Phys. **B724**, 247 (2005).

[49] S. Alioli, S.-O. Moch, and P. Uwer, Hadronic top-quark pair-production with one jet and parton showering, J. High Energy Phys. 01 (2012) 137.

[50] J. Alwall, R. Frederix, S. Frixione, V. Hirschi, F. Maltoni, O. Mattelaer *et al.*, The automated computation of tree-level and next-to-leading order differential cross sections, and their matching to parton shower simulations, J. High Energy Phys. 07 (2014) 079.

[51] T.-J. Hou *et al.*, New CTEQ global analysis of quantum chromodynamics with high-precision data from the LHC, Phys. Rev. D **103**, 014013 (2021).

[52] A. Buckley, J. Ferrando, S. Lloyd, K. Nordström, B. Page, M. Rüfenacht, M. Schönherr, and G. Watt, LHAPDF6: Parton density access in the LHC precision era, Eur. Phys. J. C **75**, 132 (2015).

[53] P. A. Zyla *et al.* (Particle Data Group Collaboration), Review of particle physics, Prog. Theor. Exp. Phys. **2020**, 083C01 (2020).

[54] J. Alwall *et al.*, A standard format for Les Houches event files, Comput. Phys. Commun. **176**, 300 (2007).

[55] T. Sjöstrand, S. Ask, J. R. Christiansen, R. Corke, N. Desai, P. Ilten *et al.*, An introduction to PYTHIA8.2, Comput. Phys. Commun. **191**, 159 (2015).

[56] P. Skands, S. Carrazza, and J. Rojo, Tuning PYTHIA8.1: The Monash 2013 tune, Eur. Phys. J. C **74**, 3024 (2014).

[57] M. Czakon, D. Heymes, A. Mitov, D. Pagani, I. Tsinikos, and M. Zaro, Top-quark charge asymmetry at the LHC and Tevatron through NNLO QCD and NLO EW, Phys. Rev. D **98**, 014003 (2018).

[58] http://powhegbox.mib.infn.it/.